Pyrazolino[60]fullerene–Oligophenylenevinylene Dumbbell-Shaped Arrays: Synthesis, Electrochemistry, Photophysics, and Self-Assembly on Surfaces

Fernando Langa,*[a] Maria J. Gomez-Escalonilla,[a] Jean-Michel Rueff,[b] Teresa M. Figueira Duarte,[b] Jean-François Nierengarten,*[b] Vincenzo Palermo,[c] Paolo Samorì,*[c, d] Yannick Rio,[c] Gianluca Accorsi,[c] and Nicola Armaroli*[c]

Abstract: Symmetrically substituted oligophenylenevinylene (OPV) derivatives bearing terminal *p*-nitrophenylhydrazone groups have been prepared and used for the synthesis of dumbbell-shaped bis(pyrazolino[60]fullerene)–OPV systems. In these triad arrays, the OPV-type fluorescence is dramatically quenched as a consequence of ultrafast OPV→C_{60} singlet energy transfer. In its turn the fullerene singlet state is quenched by pyrazoline→C_{60} electron transfer, in line with the behavior of the corresponding reference fullerene molecule. The occurrence of electron transfer in the multicomponent arrays is evidenced by recovery of fullerene fluorescence at 77 K in CH_2Cl_2 and in toluene at 298 K. Under these conditions the OPV→C_{60} energy transfer is unaffected. The rate of this process turns out to be higher for the OPV trimer than for the corresponding pentameric OPV arrays, in agreement with energy-transfer theory expectations. Scanning tunneling microscopy (STM) and scanning force microscopy (SFM) revealed that the bis(pyrazolino[60]fullerene)–OPV can self-assemble into ordered layered crystalline architectures on the basal plane of highly oriented pyrolitic graphite.

Keywords: electrochemistry · electron transfer · fullerenes · oligophenylenevinylenes · scanning probe microscopy

Introduction

Owing to its relatively low reduction potential, symmetrical shape, large size, and extended π-electron system, [60]fullerene is an ideal candidate as an electron acceptor in photo- and electroactive materials.[1,2] In particular, the electronic properties of fullerenes make them attractive in the design of new materials in which photoinduced electron transfer is the key process for the conversion of light into chemical[3] or electric energy.[4–9] The characteristics of C_{60} successfully compare with those of electron acceptors with smaller size such as benzoquinone.[1,10] Indeed, accelerated charge transfer and decelerated charge recombination have been observed in a fullerene-based donor–acceptor systems when compared to similar arrays in which C_{60} is replaced by benzoquinone.[10]

In principle, functionalization of fullerenes allows us to tune the electron-acceptor properties of C_{60} derivatives;[11,12] however, only a few C_{60} derivatives turned out to be better electron acceptors than the parent molecule.[13–16] In this regard, an important breakthrough was the synthesis of fulleropyrazolines derivatives.[17,18] The inductive effect of the pyrazoline nitrogen atom directly attached to the carbon sphere tends to make them easier to reduce than other C_{60}

[a] Prof. F. Langa, Dr. M. J. Gomez-Escalonilla
Facultad de Ciencias del Medio Ambiente
Universidad de Castilla-La Mancha, 45071 Toledo (Spain)
Fax: (+34)-925-268-840
E-mail: fernando.lpuente@uclm.es

[b] Dr. J.-M. Rueff, T. M. Figueira Duarte, Dr. J.-F. Nierengarten
Groupe de Chimie des Fullerènes et des Systèmes Conjugués
Ecole Européenne de Chimie, Polymères et Matériaux (ECPM)
Université Louis Pasteur et CNRS, 25 rue Becquerel
67087 Strasbourg Cedex 2 (France)
Fax: (+33) 3-90-242-706
E-mail: jfnierengarten@chimie.u-strasbg.fr

[c] Dr. V. Palermo, Dr. P. Samorì, Dr. Y. Rio, Dr. G. Accorsi, Dr. N. Armaroli
Istituto per la Sintesi Organica e la Fotoreattività, Consiglio Nazionale delle Ricerche, Via Gobetti 101 40129 Bologna (Italy)
Fax: (+39) 051-639-9844
E-mail: armaroli@isof.cnr.it, samori@isof.cnr.it

[d] Dr. P. Samorì
Nanochemistry Lab
Institut de Science et d'Ingénierie Supramoléculaires (I.S.I.S.)
Université Louis Pasteur, 8 allée Gaspard Monge
67083 Strasbourg (France)

 DOI: 10.1002/chem.200500089

derivatives .[12] Moreover the pyrazoline–C_{60} unit was found to act as a charge-separation module for the construction of photoactive and tunable devices.[19]

To take advantage of their original electronic properties, C_{60} and its derivatives have been linked to a variety of organic conjugated oligomers,[20] such as oligophenylenevinylenes (OPV),[19,21–26] oligophenyleneethynylene (OPE),[27] oligothiophenes (OTP),[28–31] and others.[25,32–36] These dyad and triad systems exhibit interesting intramolecular photoprocesses between the conjugated linear backbone and the carbon sphere, that is, electron or energy transfer. Some of them are used as active materials in prototype photovoltaic devices.[21,27,37] In the OPV–C_{60} arrays described so far, the desired OPV→C_{60} electron-transfer process undergoes competition from an efficient OPV→C_{60} singlet–singlet energy transfer.[21,22,24,38,39] Practically, in solution, the OPV unit acts as a light collecting (i.e., antenna) module, whilst electron transfer, the extent of which can be modulated by solvent polarity, occurs only from the lowest electronic singlet state of the C_{60} moiety.[19,40]

The exploitation of the fullerene-based molecular systems for the fabrication of optoelectronic devices requires the processing of the molecular architecture in thin films. The performance of these devices strongly depends on the interplay between electronic structure and arrangement at the supramolecular level.[41] Achieving full control of the self-assembly at surfaces of π-conjugated molecules into complex supramolecular architectures is therefore of paramount importance. Scanning probe microscopy techniques make it possible to map a surface by probing different physicochemical properties on the nano- and micrometer scale. Scanning force microscopy (SFM) and scanning tunneling microscopy (STM) studies of fullerenes have been performed on many different surfaces, at both large and small length scales. They showed the formation of layers[42] or islands of molecules, sometimes with a preferential island growth at surface step edges,[43] exhibiting hexagonal packing.[44,45] When the fullerene was linked to ferrocene, the molecule was found to physisorb on graphite into ribbons, in which the single units are packed into dimers, as ruled by the electric dipole of the molecules.[46] On the other hand, making use of the Langmuir–Blodgett technique, a C_{60} molecule functionalized with an aliphatic tail, bearing a polar head-group, was self-assembled perpendicular to the substrate producing closely spaced arrangements.[42] Thus, different types of molecular architectures have been obtained by systematically changing several parameters including the concentration of adsorbate at surface, the substrate type, and the deposition processing method and rate. Recently highly complex supramolecular architectures of fullerenes that noncovalently interact with discotic systems, such as phthalocyanine[47] or porphyrin,[48] derivatives were visualized by STM studies performed in ultra-high vacuum. Moreover, Bai and co-workers have grown electrochemically ordered nanostructures of a C_{60} derivative and a functionalized PPV, and characterized them by STM.[49]

In this paper we describe the synthesis, the electrochemistry, the photophysical properties and the self-assembly behavior in ultra-thin films of OPV–fulleropyrazoline compounds. Two of them, **F-3PV** and **F-5PV**, are dyads in which the C_{60} moiety is linked to a trimeric (**3PV**) and a pentameric (**5PV**) oligophenylenevinylene unit, respectively. The other two, **F-3PV-F** and **F-5PV-F**, are triads made of an OPV central unit (**3PV** and **5PV**) bearing a fullerene fragment at both extremities. Both the dyad and the triad systems show photoinduced energy- (OPV→C_{60}) and electron-transfer (pyrazoline→C_{60}) processes. Detailed SFM and STM studies on the largest system **F-5PV-F** reveal the spontaneous formation from solutions of highly ordered layer architectures on surfaces and, on the molecular scale, the self-assembly into polycrystalline structures characterized by a few nanometer-sized crystalline domains. A preliminary report on the preparation of **F-3PV**, **F-5PV**, **F-3PV-F**, and **F-5PV-F** was published previously.[50]

Results and Discussion

Synthesis: The strategy employed for the preparation of the C_{60}-OPV conjugates **F-3PV**, **F-5PV**, **F-3PV-F**, and **F-5PV-F** is based upon the 1,3-dipolar cycloaddition of C_{60} with bis-nitrilimine derivatives generated in a one-pot procedure from the corresponding bis-hydrazones. The synthesis of the OPV precursors bearing two hydrazone functions is shown in Schemes 1 and 2. Compound **1** was prepared in three steps from hydroquinone according to a previously reported method.[51] Reaction of **1** with 2,2-dimethylpropane-1,3-diol in refluxing benzene in the presence of a catalytic amount of *p*-toluenesulfonic acid (TsOH) gave the protected aldehyde **2** in 87% yield (Scheme 1). Subsequent treatment with

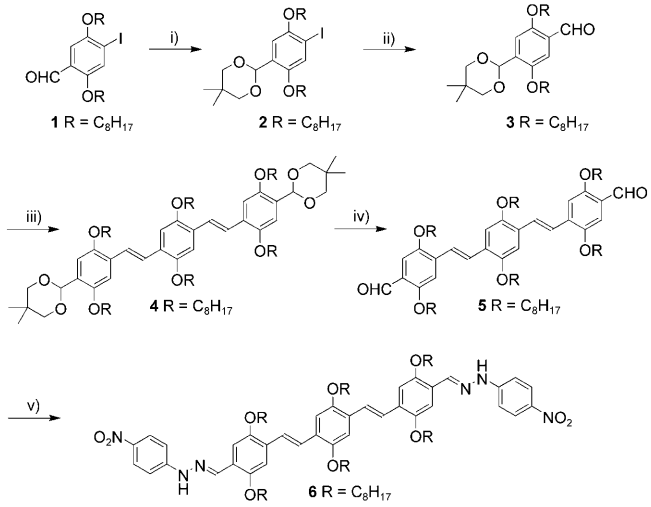

Scheme 1. Reagents and conditions: i) 2,2-dimethylpropane-1,3-diol, TsOH (cat.), benzene, Δ, Dean Stark trap, 48 h (87%); ii) *n*BuLi, Et_2O, 0°C, 1 h, then DMF, 0°C to room temperature, 4 h (86%); iii) {[2,5-bis-(octyloxy)-1,4-phenylene]bis(methylene)}bis(tetraethyl)phosphonate, *t*BuOK, THF, 0°C, 1 h, then I_2 (cat.), toluene, Δ, 12 h (80%); iv) CF_3CO_2H, CH_2Cl_2, H_2O, room temperature, 4 h (95%); v) *p*-nitrophenylhydrazine, AcOH, EtOH, Δ, 3.5 h (99%).

*n*BuLi in Et_2O at 0 °C followed by quenching with dry DMF afforded aldehyde **3** in 86 % yield. Treatment of aldehyde **3** with {[2,5-bis(octyloxy)-1,4-phenylene]bis(methylene)}bis-(tetraethyl)phosphonate[52] in THF in the presence of *t*BuOK afforded the targeted OPV trimer, but as an *E*:*Z* isomer mixture. The reaction of benzylic phosphonates with aromatic aldehydes under Wittig–Horner conditions is generally stereoselective, leading to the *E* isomer only. In the present case, steric hindrance resulting from the presence of the octyloxy group in the *ortho*-position of the reactive groups in both reagents may explain the lack of *E*:*Z* selectivity. Isomerization to the all-*E* derivative **4** was easily achieved by treatment with a catalytic amount of iodine in refluxing toluene and trimer **4** was thus obtained in 80 % yield. Subsequent deprotection with CF_3CO_2H in CH_2Cl_2/H_2O afforded bis-aldehyde **5** in 95 % yield. The *E* configuration of the double bonds in **5** was confirmed by a coupling constant of about 17 Hz for the AB system corresponding to the vinylic protons in the ^1H NMR spectrum. Bis-hydrazone **6** was then obtained in 99 % yield from aldehyde **5** and *p*-nitrophenylhydrazine in refluxing ethanol in the presence of acetic acid.

The preparation of the corresponding OPV pentamer **12** is depicted in Scheme 2. $LiAlH_4$ reduction of aldehyde **3**

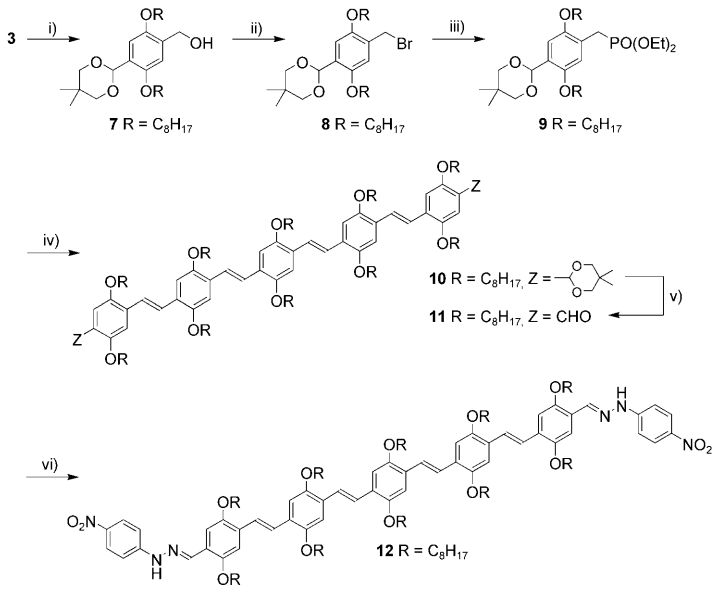

Scheme 2. Reagents and conditions: i) $LiAlH_4$, THF, 0 °C, 4 h (80 %); ii) CBr_4, PPh_3, THF, 0 °C to room temperature, 4 h (85 %); iii) $P(OEt)_3$, 150 °C, 4 h (99 %); iv) **5**, *t*BuOK, THF, 0 °C to room temperature, 2 h, then I_2 (cat.), toluene, Δ, 12 h (51 %); v) CF_3CO_2H, CH_2Cl_2, H_2O, room temperature, 3 h (88 %); vi) *p*-nitrophenylhydrazine, AcOH, EtOH, Δ, 3.3 h (83 %).

yielded alcohol **7** which, after treatment with CBr_4/PPh_3, gave bromide **8**. Phosphonate **9** was then obtained in 99 % yield by reaction of **8** with triethylphosphite under Michaelis–Arbuzov conditions. Reaction of bis-aldehyde **5** with phosphonate **9** under Wittig–Horner conditions, followed by treatment with a catalytic amount of iodine in refluxing toluene gave the all-*E* OPV pentamer **10** in 51 % yield. Deprotection, accomplished by treatment with CF_3CO_2H in CH_2Cl_2/H_2O, followed by reaction of the resulting bis-aldehyde **11** with *p*-nitrophenylhydrazine in refluxing ethanol in the presence of acetic acid, afforded bis-hydrazone **12** in 83 % yield.

Bis-hydrazones **6** and **12** were characterized by analytical and spectroscopic data (see Supporting Information for details). The ^1H NMR spectra of both compounds confirm the *E* configuration of the double bonds by a coupling constant of approximately 17 Hz for the AB system corresponding to the vinylic protons. Also, their structures were confirmed by MALDI-TOF mass spectra, which show the expected $[M+H]^+$ peaks at $m/z = 1376.8$ (**6**) and 2094.2 (**12**).

Treatment of bis-hydrazone **6** with *N*-chlorosuccinimide (NCS) and pyridine in dry chloroform, followed by reaction of the resulting bis-nitrilimine intermediate with C_{60} in chlorobenzene in the presence of Et_3N at room temperature afforded the desired dumbbell-shaped derivative **F-3PV-F** in 27 % yield (Scheme 3). Interestingly, in addition to **F-3PV-F**,

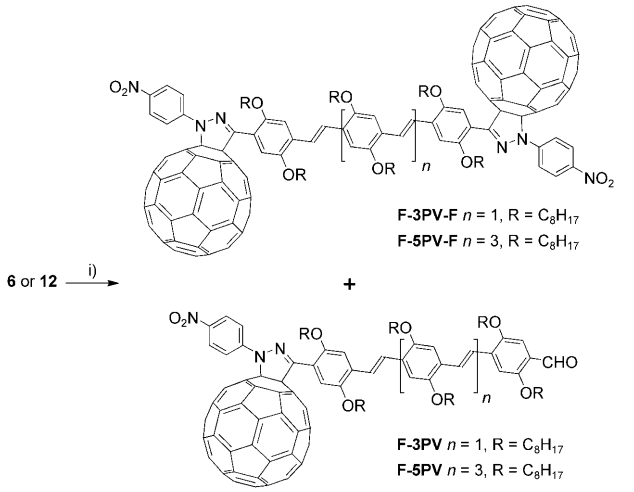

Scheme 3. Reagents and conditions: i) NCS, pyridine, $CHCl_3$, 0 °C to room temperature, then C_{60}, Et_3N, chlorobenzene, room temperature, 1 h (from **6**: **F-3PV-F** (27 %) and **F-3PV** (58 %); from **12**: **F-5PV-F** (10 %) and **F-5PV** (19 %)).

the monosubstituted derivative **F-3PV** was also isolated from the reaction mixture; the aldehyde group in **F-3PV** probably originated by hydrolysis of unreacted hydrazone moiety during the workup procedure. Following the same procedure, the reaction of bis-hydrazone **12** with NCS and subsequent reaction with C_{60} at room temperature gave the bis-(pyrazolino[60]fullerene) OPV derivative **F-5PV-F** and the monosubstituted compound **F-5PV** in 10 and 19 % yields, respectively.

Owing to the presence of the octyloxy groups, the C_{60}–OPV conjugates[50] **F-3PV**, **F-5PV**, **F-3PV-F**, and **F-5PV-F** are well soluble in common organic solvents (CH_2Cl_2, $CHCl_3$, benzene, toluene, THF) and were thus easily characterized by UV-visible, FT-IR, and ^1H and ^{13}C NMR spectros-

copy (see Supporting Information). The structures of the four C_{60}–OPV arrays were also confirmed by their MALDI-TOF mass spectra showing the expected molecular ion peaks in each case (*m/z*): 2814.7 (**F-3PV-F**), 3530.9 (**F-5PV-F**), 1959.8 (**F-3PV**), and 2676.5 (**F-5PV**).

The fulleropyrazoline and OPV derivatives shown here have been also prepared. They were used as reference com-

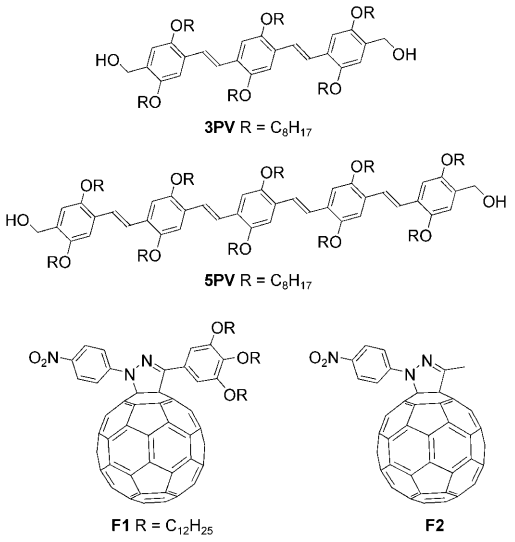

pounds for multicomponent arrays in the photophysical investigations. Compounds **F1** and **F2** were prepared as previously reported.[19,53] The OPV derivatives **3PV** and **5PV** were obtained by $LiAlH_4$ reduction of the corresponding bis-aldehydes **5** and **11**, respectively.

Electrochemistry: The electrochemical behavior of bis-hydrazones **6** and **12**, dyads **F-3PV** and **F-5PV** and triads **F-3PV-F** and **F-5PV-F** was investigated by cyclic voltammetry (CV) and Osteryoung square-wave voltammetry (OSWV) techniques at room temperature in ODCB/CH_3CN (4:1) as solvent (ODCB = *ortho*-dichlorobenzene) and using $Bu_4N^+ ClO_4^-$ (TBAP) as the supporting electrolyte. The redox potentials **F-3PV**, **F-5PV**, **F-3PV-F**, and **F-5PV-F** are reported in Table 1 and are compared to those of the precursors **6** and **12**, and pristine C_{60} as reference. The cyclic voltammogram of **F-3PV-F** is depicted in Figure 1.

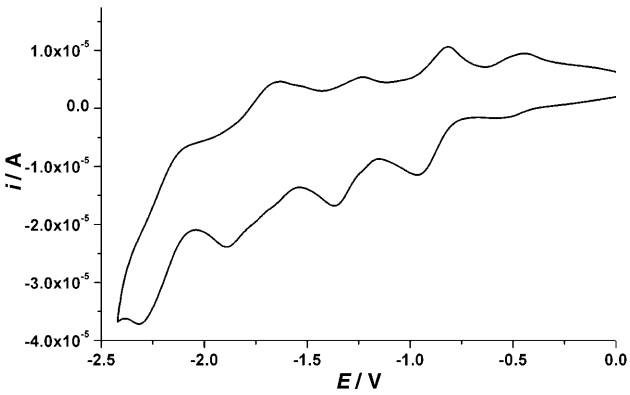

Figure 1. Cyclic voltammogram of compound **F-3PV-F**.

As a general feature on the reduction side, triads **F-3PV-F** and **F-5PV-F** give rise to six one-electron reduction waves. Four of them (E^1_{red}, E^2_{red}, E^4_{red}, and E^6_{red}) are quasi-reversible and correspond to the successive reductions of the fullerene core. The other two waves are irreversible and the peaks E^3_{red} and E^5_{red} are assigned to the reduction of the *p*-nitrophenyl moiety by comparison with the model compounds **6** and **12**. Comparable electrochemical behavior is shown by **F-3PV** and **F-5PV**. Similar to other pyrazolino[60]fullerene derivatives, the first reduction potentials (E^1_{red}) are analogous to that of pristine C_{60} and shifted to more positive values relative to other fullerene derivatives due to the $-I$ effect of the pyrazoline ring.[53,54]

On the oxidation side, an irreversible one-electron wave was observed at around +0.44 V (**F-3PV-F**) and +0.35 V (**F-5PV-F**), while these waves appear at +0.34 V and +0.31 V in **F-3PV** and **F-5PV**, respectively. Similarly, bis-hydrazones **6** and **12** show the same oxidation around +0.37 V. These values can be assigned to the oxidation of the OPV moiety, in agreement with previous reports.[19] The second oxidation wave in the two bis-hydrazones must be attributed to the hydrazone moiety;[53] an additional wave is observed in **F-3PV** and **F-5PV** at around +0.6 V, assigned to the oxidation of the aldehyde group.

As support for the electrochemical results, the structures of both dimers, **F-3PV-F** and **F-5PV-F**, were calculated at the semiempirical PM3 level.[55] This revealed torsion angles of ~38° between the *p*-nitrophenyl moiety and the pyrazolino rings, thus preventing conjugation between them, whereas the OPV unit and the pyrazoline rings are almost coplanar (the dihedral angle is lower than 10°; see Figure 2). The LUMO levels of both dumbbell compounds were found to be lower than that of C_{60}; these calculations confirmed the experimentally determined first reduction potential in **F-3PV-F** and **F-5PV-F**. As expected, the

Table 1. Redox potentials (OSWV) of organofullerenes **F-3PV-F**, **F-5PV-F**, **F-3PV**, **F-5PV**, bis-hydrazones **6** and **12**, and C_{60}.[a]

Compound	E^1_{red}	E^2_{red}	E^3_{red}	E^4_{red}	E^5_{red}	E^6_{red}	E^1_{ox}	E^2_{ox}	E^3_{ox}
F-3PV-F	−0.95	−1.37	−1.71[b]	−1.84	−2.09[b]	−2.27	+0.44[c]	–	–
F-5PV-F	−0.94	−1.37	−1.70[b]	−1.87	−2.07[b]	−2.25	+0.35[c]	–	–
F-3PV	−0.96	−1.39	−1.70[b]	−1.86	−2.02[b]	−2.21	+0.34[c]	+0.61[c]	–
F-5PV	−0.99	−1.40	−1.72[b]	−1.85	−2.06[b]	−2.32	+0.31[c]	+0.62[c]	–
6	–	–	−1.67[b]	–	−2.09[b]	–	+0.38[c]	–	+1.17[c]
12	–	–	−1.69[b]	–	−2.06[b]	–	+0.37[c]	–	+1.18[c]
C_{60}	−0.97	−1.38	–	−1.85	–	−2.31	–	–	–

[a] V vs $Ag/AgNO_3$; GCE as working electrode; 0.1 M TBAP; ODCB:MeCN (4:1); scan rate: 100 mV s^{-1}. [b] Irreversible according to CV. [c] Measured by CV.

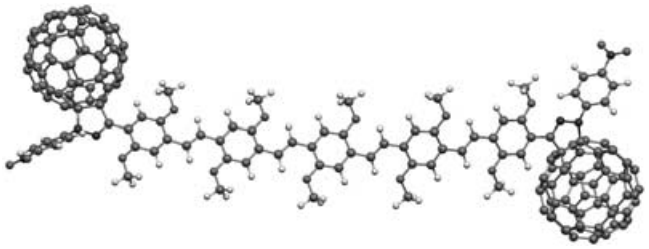

Figure 2. Most stable conformation of **F-5PV-F**. The $-OC_8H_{17}$ groups have been replaced by $-OCH_3$ groups for calculations.

HOMO is centered in the OPV unit and the LUMO is shared between the two C_{60} cages.

As shown in Table 2, and in line with the electrochemical data, the calculated HOMO–LUMO gap is smaller than that of C_{60}. This gap is significantly lower in the **5PV** system (**F-5PV-F**) than in the **3PV** derivative (**F-3PV-F**), suggesting the possibility of an easier electron transfer process.

Table 2. Calculated (PM3) HOMO and LUMO levels of **F-3PV-F**, **F-5PV-F**, and C_{60}.

	E_{HOMO} [eV]	E_{LUMO} [eV]	ΔE [eV]
F-3PV-F	−8.32	−3.13	5.19
F-5PV-F	−7.84	−3.06	4.78
C_{60}	−9.48	−2.88	6.60

Photophysical properties

Fullerene and OPV model compounds: Fulleropyrazoline **F1** undergoes intramolecular electron transfer from the lone pair of the pyrazoline sp^3 nitrogen atom to the carbon sphere.[19] This process, which is signalled by the dramatic quenching of the typical fullerene-type fluorescence around 700 nm, can be suppressed in acid solution in which the protonation of the sp^3 nitrogen lone pair prevents electron migration.[19] However, it is interesting to point out the crucial role played by the tridodecyloxybenzene unit attached to the heteroatomic five-membered ring. In fact if one takes the fulleropyrazoline **F2**, bearing a methyl rather than a phenyl group as a peripheral unit, electron transfer is no longer observed and the fullerene fluorescence is restored. Both **F1** and **F2** exhibit virtually identical absorption spectra, but **F2** is a stronger emitter with a fluorescence quantum yield of 5.0×10^{-4} in CH_2Cl_2 (Table 3). This value is quite similar to that of fulleropyrrolidines,[38] which are among the strongest emitters within the family of monosubstituted fullerenes.

The different behavior between **F1** and **F2** can be rationalized by some degree of delocalization of the positive charge, upon oxidation, provided by the tridodecyloxybenzene ring of **F1**. This result is in agreement with those observed in other fulleropyrazoline derivates with electron-donor or electron-withdrawing susbtituents.[54]

The absorption spectra of the oligophenylenevinylene (OPV) model compounds **3PV** and **5PV** are depicted in Figure 3. They exhibit the characteristic π–π^* absorption with maxima at 409 and 447 nm, respectively. The maximum of the more extended π-conjugated **5PV** lies at lower energy relative to **3PV** and exhibits a higher molar extinction coefficient, as a result of the larger number of phenyl rings.[19,22]

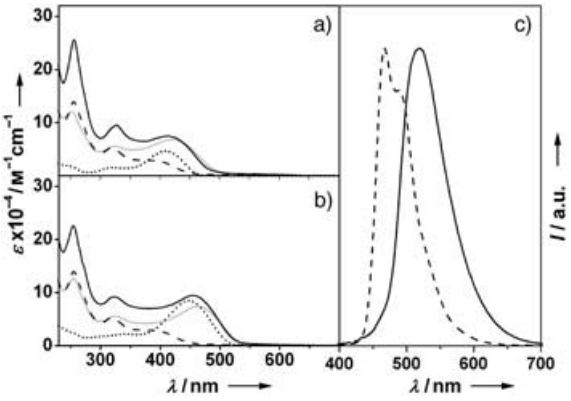

Figure 3. Electronic absorption spectra in CH_2Cl_2 of: a) **3PV** (black dotted line), **F-3PV** (grey full line), **F-3PV-F** (black solid line) and **F1** (black dashed line). b) **5PV** (black dotted line), **F-5PV** (grey full line), **F-5PV-F** (black full line) and **F1** (black dashed line). c) Fluorescence spectra of **3PV** (black dashed line) and **5PV** (black full line); CH_2Cl_2, $\lambda_{exc}=320$ nm, $A=0.15$.

Table 3. Fluorescence properties[a] and excited state singlet lifetimes in CH_2Cl_2.

	OPV moiety (298 K)			C_{60} moiety (298 K)			OPV moiety (77 K)		C_{60} moiety (77 K)	
	λ_{max} [nm][b]	Φ_{fl}[b]	τ [ns][c]	λ_{max} [nm][d]	Φ_{fl}[d]	τ [ns][c]	λ_{max} [nm][b]	τ [ns][c]	λ_{max} [nm][d]	τ [ns][c]
F1	–	–	–	706	$\leq$0.00001	–[e]	–	–	698	1.5
F2	–	–	–	706	0.00055	1.5	–	–	710	1.5
3PV	466	0.64	1.5	–	–	–	504	1.4, 5.0	–	–
F-3PV	526	0.00026	–[f]	706	$\leq$0.00001	–[e]	516	–[f]	696	1.7[g]
F-3PV-F	480	0.00007	–[f]	706	$\leq$0.00001	–[e]	516	–[f]	694	2.2[g]
5PV	526	0.35	1.2	–	–	–	600	0.7, 2.5	–	–
F-5PV	580	0.00170	–[f]	706	$\leq$0.00001	–[e]	–[h]	–[h]	690	1.3[g]
F-5PV-F	570	0.00025	–[f]	706	$\leq$0.00001	–[e]	–[h]	–[h]	690	1.2[g]

[a] From emission spectra corrected for the photomultiplier response. [b] Excitation on the maximum of the OPV absorption band (see Figures). [c] $\lambda_{exc}=407$ nm. [d] $\lambda_{exc}=600$ nm. [e] Not measured due to signal weakness. [f] Below the temporal resolution of our apparatus (200 ps); see text for an estimation of these lifetimes based on Equation (1). [g] $\lambda_{em}=800$ nm, very weak and noisy signal due to low photomultiplier sensitivity and poor quality of the rigid matrix. [h] Indistinguishable over the instrumental noise.

Some relevant photophysical data are collected in Table 3. Model compound **3PV** exhibits an intense fluorescence band (Figure 3) in CH_2Cl_2 both at 298 K ($\lambda_{max}=466$ nm, $\varphi_{fl}=0.64$) and at 77 K ($\lambda_{max}=504$ nm). The singlet decay time is monoexponential at room temperature ($\tau=1.5$ ns), whereas at 77 K a biexponential decay is observed ($\tau_1=1.4$ ns, $\tau_2=5.0$ ns), probably as a consequence of the presence of two different frozen rotameric forms in the solid matrix.[21,56] The fluorescence properties of **5PV** in CH_2Cl_2 are similar to **3PV**. An intense emission band is observed both at room temperature ($\lambda_{max}=526$ nm , $\varphi_{fl}=0.35$, $\tau=1.2$ ns; Figure 3) and at 77 K in a rigid matrix ($\lambda_{max}=564$ nm, $\tau_1=0.7$ ns, $\tau_2=2.5$ ns). The comparison of the fluorescence properties of **3PV** and **5PV** leads to the same observations described for other similar systems: the singlet excited-state lifetime and the photoluminescence quantum yield decrease with increasing conjugation length.[57]

*Dimeric compounds **F-3PV** and **F-5PV***: The absorption spectra of **F-3PV** and **F-5PV** are shown in Figure 3. If one compares them with the sum of the spectra of the component units (**F**, **3PV**, **5PV**) some differences can be noticed; in particular a red-shift of the OPV absorption band is found. This difference is likely to be due to the more extended π-conjugation of the OPV-type moiety in **F-3PV** and **F-5PV** compared to **3PV** and **5PV**, which possess CH_2OH terminal groups.

For any dyad, it is not possible to excite either the C_{60} or the OPV moiety with 100% selectivity (Figure 3). Nevertheless, most of the light is absorbed by the OPV unit when exciting in the range 450–520 nm. On the other hand, a substantial part of the light is absorbed by the fullerene moiety for $\lambda<350$ nm and $\lambda>630$ nm, at which it exhibits a very weak absorption tail, ($\varepsilon\sim300\,M^{-1}\,cm^{-1}$ at 650 nm).[19]

The OPV-type fluorescence bands of **F-3PV** and **F-5PV** are both red-shifted (as the absorption spectra) and dramatically quenched relative to **3PV** and **5PV** (Table 3). Upon excitation at 470 nm, at which the OPV moiety prominently absorbs, a 2400- and 210-fold fluorescence intensity decrease is observed relative to the model compounds **F-3PV** and **F-5PV**, respectively. In **F-3PV** and **F-5PV** sensitization of the fullerene fluorescence cannot be used as a probe for OPV→C_{60} energy transfer, as done earlier for similar dyads containing fulleropyrrolidines.[21] In the present case, as pointed out above, the fullerene fluorescence is intrinsically quenched by intramolecular electron transfer from the pyrazoline group to the carbon sphere. Practically, in CH_2Cl_2 both the potentially fluorescent moieties are quenched at room temperature in **F-3PV** and **F-5PV**. The very weak fluorescence band observed for the reference fullerene **F1** (Table 3) is completely obscured by the tail of the residual OPV emission when excitation is addressed to the OPV moiety. On the other hand, excitation of the C_{60} subunits results in a very weak fluorescence band, identical to those of **F1** (Table 3). In analogy with a similar fulleropyrazoline–C_{60} array investigated earlier,[19] we assume that ultrafast quenching of the OPV moiety in **F-3PV** and **F-5PV** is due to singlet energy transfer to the carbon sphere, which, once excited, undergoes pyrazoline→C_{60} electron transfer. The lack of fullerene sensitization is also confirmed by NIR luminescence. We could not observe any sensitized singlet oxygen emission at 1270 nm for **F-3PV** and **F-5PV**, confirming the lack of fullerene triplet formation.[19]

The occurrence of intramolecular electron transfer in **F-3PV** and **F-5PV**, in line with the behavior of the reference molecule **F1**, is supported by the recovery of the fluorescence in CH_2Cl_2 at 77 K (Table 3, Figure 4) and in a less

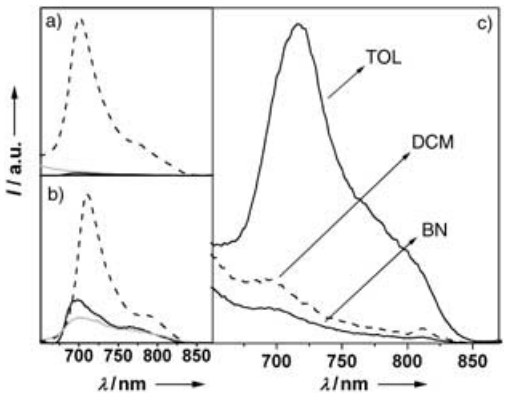

Figure 4. Fluorescence spectra of **F-3PV** (black full line), **F1** (grey full line) and **F2** (black dashed line) in: a) 298 K, CH_2Cl_2, solution; b) 77 K, CH_2Cl_2, rigid matrix. c) Fluorescence spectra of **F-3PV** in solvents of different polarity, toluene (TOL), dichloromethane (DCM) and benzonitrile (BN). For all compounds $\lambda_{exc}=330$ nm and $A=0.80$.

polar solvent as toluene at 298 K (Figure 4). Under these conditions the solvent repolarization around the charge-separated couple is prevented or strongly limited, thus disfavoring the electron-transfer process.

However, under these same conditions, quenching of the OPV fluorescence is still active. This provides evidence for two distinct photoprocesses in **F-3PV** and **F-5PV**, such as OPV→C_{60} energy transfer and pyrazoline→C_{60} electron transfer, for which the latter can be controlled by temperature and solvent polarity.[19] From Equation (1)[22] it is possible to estimate the rate constant of the OPV→C_{60} energy-transfer process, which turns out to be 1.6×10^{12} and $1.7\times10^{11}\,s^{-1}$, corresponding to OPV quenched lifetimes of 0.6 and 5.9 ps respectively, that is, below our instrumental resolution. In Equation (1), Φ and Φ_{ref} are the OPV fluorescence quantum yield of the multicomponent arrays and of the reference compounds, whereas τ_{ref} is the singlet lifetime of the latter.

$$k_{EnT}=\frac{(\Phi_{ref}/\Phi)-1}{\tau_{ref}} \quad (1)$$

*Trimeric compounds **F-3PV-F** and **F-5PV-F***: The absorption spectra of **F-3PV-F** and **F-5PV-F** in CH_2Cl_2 are reported in Figure 3. Similarly to the dimeric systems, a red-shift

of the OPV moiety absorption band is observed for **F-3PV-F** and **F-5PV-F** with respect to the OPV model compounds **3PV** and **5PV**, which can be rationalized as for the dyads (see above).

The excited state behavior of **F-3PV-F** and **F-5PV-F** in CH_2Cl_2 is practically the same as the dyad analogues. In particular we observe: 1) strong quenching of the OPV fluorescence in solvents of any polarity due to OPV→C_{60} energy transfer, 2) quenching of fullerene fluorescence, 3) recovery of C_{60} fluorescence by cooling down the samples to 77 K, 4) recovery of fullerene fluorescence by decreasing the solvent polarity (toluene), 5) no substantial effects of solvent polarity on the extent of OPV fluorescence quenching, and 6) no evidence of formation of fullerene triplet under any condition. These results suggest the occurrence of OPV→C_{60} energy transfer and pyrazoline→C_{60} electron transfer for **F-3PV-F** and **F-5PV-F**.

The quenching factors for the OPV fluorescence band in the triads are 9600 and 1400 for **F-3PV-F** and **F-5PV-F**, respectively. According to Equation (1), the rate of energy transfer (k_{EnT}) can be calculated as 6.4×10^{12} and 1.1×10^{12} s^{-1}, respectively, corresponding to lifetimes shorter than 1 ps. It is interesting to note (see Table 3) that OPV→C_{60} singlet energy transfer, signaled by OPV fluorescence quenching, is more efficient for the pentameric rather than the trimeric OPV (see **F-5PV-F** vs **F-3PV-F** and **F-5PV** vs **F-3PV**) and also on increasing the number of fullerenes units (see **F-3PV** vs **F-3PV-F** and **F-5PV** vs **F-5PV-F**). These results can be rationalized in terms of energy-transfer theory both under the Förster and the Dexter approach, which can be applied for OPV–C_{60} arrays as already discussed.[21] In this frame the energy-transfer rate is increased upon enlargement of the overlapping area between the emission spectra of the sensitizer (OPV in our case) and the absorption spectra of the quencher (C_{60}). As shown in Figure 3, the molar extinction coefficient of fulleropyrazoline constantly decreases above 400 nm, while, on the other hand, the OPV fluorescence bands are red-shifted when increasing the conjugation length. As a consequence, the overlap integral is larger for **3PV**- than **5PV**-based systems and increases by passing from one to two fullerene units. Accordingly, the quenching factor is the highest for **F-3PV-F** and the smallest for **F-5PV**, corresponding to a 40-fold difference in the k_{EnT} value.

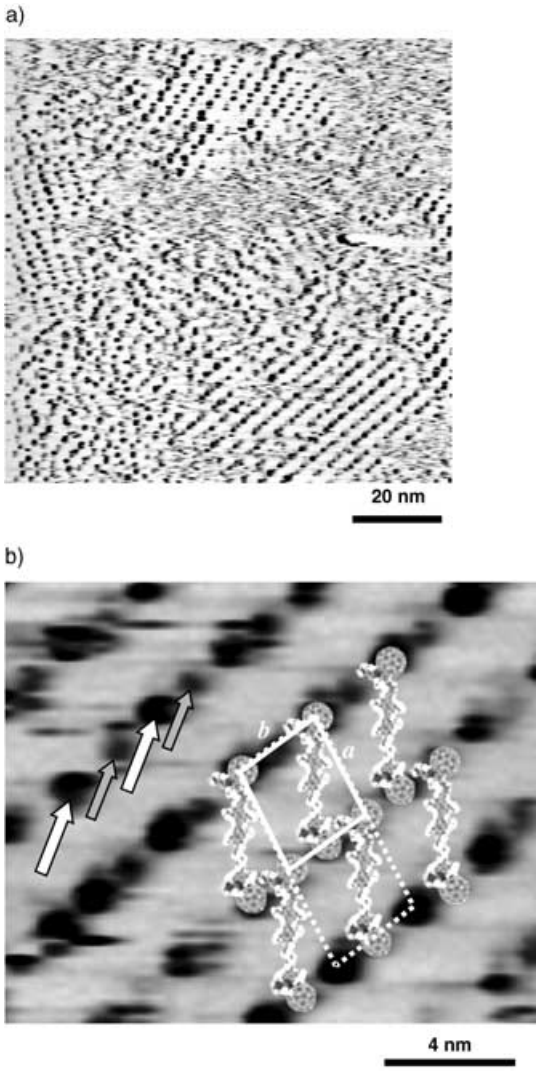

Figure 5. a) STM current images of **F-5PV-F** physisorbed at the solution–HOPG interface. b) Zoom-in of a monocrystalline area. Arrows indicate dark spots, which are ascribed to fullerenes. Molecule shape and dimensions have been obtained from energy minimization of a single isolated molecule using commercial software. For sake of clarity, the alkyl chains are not shown. The 1×1 unit cell is drawn with a solid line and the 2×1 superstructure with a dashed line. Tunneling parameters: Tip bias (U_{tip}) = 550 mV, average tunnelling current (I_t) = 15 pA.

STM and SFM investigations of F-5PV-F at surfaces: An STM study at the solid–liquid interface made it possible to cast light onto the self-assembly on highly oriented pyrolitic graphite (HOPG) with a nanometer scale resolution. Figure 5a displays an STM current image recorded at the solid–liquid interface. It shows a polycrystalline structure characterized by small crystalline domains. The limited size of the crystals, being in the range of a few tens of square nanometers, can be explained in view of the competition between the tendency of the OPV to assemble on HOPG[58] and the poor inclination of C_{60} to pack on graphite[59] at the solid–liquid interface. In Figure 5b a zoom-in showing a single 2D crystal is depicted. The unit cell of the packing was determined from 2D Fourier analysis as $a=3.2\pm0.2$ nm $b=2.7\pm0.2$ nm, and $\alpha=79\pm4°$ and confirmed by auto-correlation averaging (see the Supporting Information). Molecular mechanics modeling revealed a molecular length of ~4.5 and a width of 2.2 nm, in the case in which both the OPV chain and the alkyl side chains adopt a fully extended conformation.

Usually, in STM current images the bright areas (corresponding to high tunnelling current) can be ascribed to the π-conjugated part of the molecule, since the energy difference between their frontier orbital and the Fermi level of the substrate is relatively small.[60] In the present case semi-

empirical PM3 calculations performed with Hyperchem 5.1 revealed a distribution of the electronic states (HOMO and LUMO) as reported in Figure 6. These levels need to be correlated with the Fermi level of HOPG which amounts to −4.7 eV.

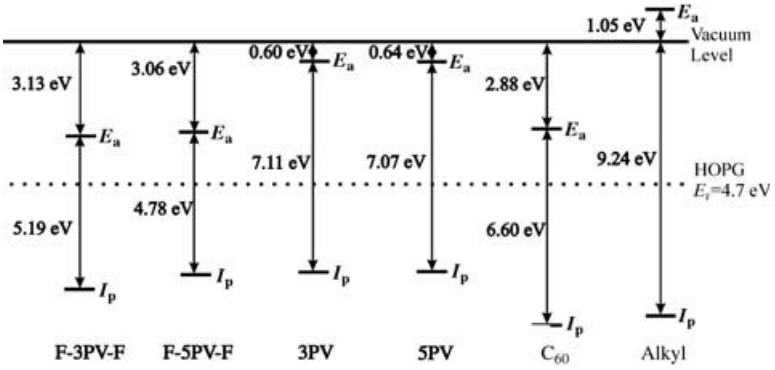

Figure 6. Scheme of the electron affinities (E_a) and ionization potential (I_p) for different molecular systems (**F-3PV-F** and **F-5PV-F**) and moieties (**3PV**, **5PV**, C_{60}, alkyl chains) in vacuum as estimated with semiempirical calculations in vacuo. Since the experimental results have been recorded in the condensed phase, for the interpretation of the STM contrasts they have to be considered only for the trend in the energy differences of the levels.

By recording STM current images with a tunneling tip that has a positive polarity, the obtained contrast is mainly dominated by the HOMO of the adsorbate. Therefore one should expect a brighter contrast for the oligo-PV segment, a darker one for the alkyl chains, and an even darker one yet for the C_{60} moiety. The black circles in the STM images, marked with white arrows in Figure 5b, have sizes similar to the fullerene moiety.

Correlating the STM measurements obtained in a monocrystalline areas with the results of molecular modeling, we propose a molecular packing as the one depicted in Figure 5b. The dark spots can be ascribed to the fullerene moieties, while the OPV segments are tilted respect to the fullerene rows.

While both the Fourier analysis and the auto-correlation averaging yielded the dimension of the smaller lattice cell, that is, 3.2×2.7 nm, careful observation of the STM images revealed the presence of smaller dark spots alternated with the bigger ones along the C_{60} rows, as marked in Figure 5b with grey and white arrows, respectively. Given the size of the unit cell and the type of contrast observed in Figure 5, one model of packing can be proposed. This is based on the consideration that the *b* vector spacing of 2.7 nm is filled with two fullerenes in a row. This distance is larger than twice the 1.004 nm hard-sphere diameter of fullerenes.[61] This might be explained with the effect of the steric hindrance of the nitro-functionalized pyrazoline linked to the C_{60}. The thermodynamically favored interactions between two electron acceptors,[62] such as nitro and fullerene, could promote the co-adsorption of neighboring C_{60} and NO_2 units along the dark rows, leading to the observed spacing of 2.7 nm.

In this case the different contrast of the two adjacent C_{60} groups could be due to the different distance of the molecule from the substrate along the *z* axis. In view of this interpretation, a 2×1 superstructure describes correctly the supramolecular motif, whereby the correct unit cell bridges four equivalent larger dark spots, as indicated with a dashed line in Figure 5b. In other words, the rows parallel to the *b* vector of the unit cell consist of a periodic structure which conveys two C_{60} moieties packed at the same height from the surface that are intercalated by a third C_{60} moiety slightly shifted vertically with respect to the two neighboring ones. This packing motif allows a reducion in the steric hindrance, similar to the case of the supramolecular staircase of functionalized hexa-*peri*-hexabenzocoronene films observed by STM at the graphite–solution interface.[63] Unfortunately the spatial resolution attained here in the STM imaging did not allow us to elucidate the packing at the molecular scale of the PV moieties and the alkyl chains. This is due to the high conformational mobility at surfaces as reflected by the small size of the crystalline domains.

The SFM measurements at the solid–air interface allowed us to study molecular packing on the (sub-)micrometer scale. Figure 7 displays topographical images of a dry film of **F-5PV-F** prepared by drop-casting a 5×10^{-3} mg mL^{-1} solution of the sample in toluene on HOPG. It reveals a self-assembled layer of **F-5PV-F** extended on the micrometer scale. It conveys holes with various lateral sizes, that is, from one micrometer down to a few nanometers. Tracing topographical profiles across these holes it was possible to determine the film thickness as 1.3 nm. Taking into account the 1.004 nm hard-sphere diameter of fullerene,[61] the measured thickness does not correspond to a single nor to a double layer, but rather indicates that, due to the tight packing, not all the fullerenes moieties are at the same height on graphite, but that some of them are shifted vertically, in good agreement with the 2×1 supramolecular pattern model described above.

The layer structure on the micron scale appears similar to that obtained from the assembly on mica of a fullerene molecule in which the bulky ball is linked to an aliphatic chain with a terminal carboxyl unit.[42] Nevertheless the two cases are different. The one described in Langmuir–Blodgett processing of the molecules on the hydrophilic mica surface[42] gave an edge-on packing, with the aliphatic chains arranged perpendicular to the basal plane of the surface, giving a 3 nm thick layer. In contrast, in the system studied here, the molecules lie flat on the graphite surface forming the self-as-

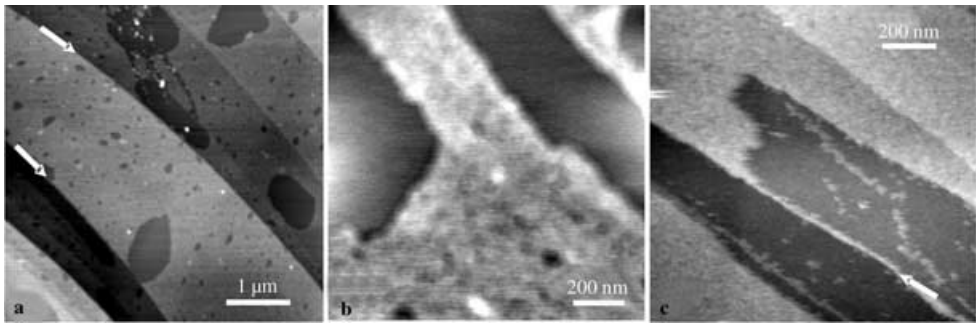

Figure 7. a,b) SFM images of **F-5PV-F** in toluene, 5×10^{-3} mg mL^{-1} showing a self-assembled layer adsorbed on the graphite. White arrows indicate graphite steps on the surface. c) Anisotropic molecular ad-layer adsorbed at a graphite step, indicated by an arrow. *z* ranges : a) 12 nm; b) 3.4 nm; c) 5.5 nm.

sembled layer. Because of the limit in the resolution of non-contact mode SFM being on the order of a few nanometers, one cannot identify within the layer the different thickness of the central backbone of the molecule and the side groups of the C_{60} moieties. Whilst the overall root-mean square roughness (R_{rms}) of this film over areas of 1×1 μm is very small (~1.5 nm), on the nanometers scale it is governed by the different moieties that comprise the single molecule.

The boundaries in the self-assembled monolayers (indicated by white arrows in Figure 7a) are dictated by the structure of the crystalline HOPG underneath. In some lower coated areas of the surface, a preferential adsorption at the step edges has been observed, forming long thin molecular rows (arrow in Figure 7c) with widths of tens of nanometers. A more diluted solution (5×10^{-5} mg mL^{-1}) leaded to an adsorbed layer similar to that described above, but with larger holes (images not shown).

The self-assembled layer extended on the scale of several micrometers provides evidence for the strong tendency of the molecules to aggregate due to π–π stacking.[64] As the growth of such ordered films of π-conjugated molecules on graphite is a kinetically controlled process,[65] a higher degree of order was achieved exploiting a slow deposition process such as drop casting, when compared to the less-ordered thin films produced by spin coating a similar hybrid molecular system.[21] The paramount role played by π–π interactions in the self-assembly of **F-5PV-F** at surfaces was evidenced also by the tendency of films prepared from a more concentrated solution to give large disordered agglomerates with diameters of hundreds of nanometers (images not shown).

Conclusion

Symmetrically substituted oligophenylenevinylene (OPV) derivatives bearing terminal *p*-nitrophenyl-hydrazone groups have been prepared and used for the synthesis of dumbbell-shaped bis(pyrazolino[60]fullerene)–OPV systems with one (**F-3PV**, **F-5PV**) or two (**F-3PV-F**, **F-5PV-F**) C_{60} terminal units. All of these arrays exhibit intramolecular OPV→C_{60} energy transfer and pyrazoline→C_{60} electron transfer. The former process, signaled by quenching of the OPV moieties, is the fastest for **F-3PV-F** and the slowest in the case of **F-5PV**, in agreement with energy-transfer theory predictions.

A fine tuning of the processing conditions from solutions allowed the production of ordered layer architectures of the **F-5PV-F** on HOPG surfaces. An SFM study at the solid–air interface revealed a pretty smooth surface in the micrometer scale. On the other hand, molecular scale explorations performed with STM have shown the tendency of this hybrid molecular system to form polycrystalline structures characterized by very small crystalline domains. This can be explained in view of the competition between physisorption at surfaces and solvation of the different units composing the molecule.

Experimental Section

General: Reagents and solvents were purchased as reagent grade and used without further purification. The preparation of compounds **1**–**12** is described in the Supporting Information. All reactions were performed in standard glassware under an inert Ar atmosphere. Evaporation and concentration were done at water aspirator pressure and drying in vacuo at 10^{-2} Torr. Column chromatography: silica gel 60 (230–400 mesh, 0.040–0.063 mm) was purchased from E. Merck. Thin-layer chromatography (TLC) was performed on glass sheets coated with silica gel 60 F_{254} purchased from E. Merck, visualization by UV light. NMR spectra were recorded on a Bruker AC 200 (200 MHz) or a Bruker AM 400 (400 MHz) with solvent peaks as reference. Mass measurement were carried out on a Brucker BIFLEX™ matrix-assisted laser desorption time-of-flight mass spectrometer (MALDI-TOF). A saturated solution of 1,8,9-trihydroxyanthracene (dithranol ALDRICH EC: 214–538–0) in CH_2Cl_2 was used as a matrix. FAB mass spectra were obtained on a VG AutoSpec instrument, using *m*-nitrobenzyl alcohol as a matrix. FT-IR spectra were recorded on a Nicolet Impact 410 spectrophotometer using KBr disks. Elemental analyses were performed by the analytical service at the Institut Charles Sadron, Strasbourg.

General procedure for the preparation of the C_{60}-OPV derivatives: Pyridine (5 μL) was added under argon to a solution of the appropriate hydrazone (1 equiv) in dry chloroform (10 mL). The mixture was cooled to 0 °C, NCS (4.1 equiv) was added, and the mixture was stirred for 1 hour; [60]fullerene (2.2 equiv) in dry chlorobenzene (30 mL) and Et_3N (1 equiv) were then added. The solution was allowed to reach room temperature and stirred for 1 hour. The solvent was removed under reduced pressure and the two reaction products were purified by silica gel flash

chromatography, with toluene as eluent. Centrifugation with methanol (4 times) achieved further purification of the solid.

F-3PV-F: Yield: 27%; ^{1}H NMR ($CDCl_3$): δ=8.34 (d, J=9.5 Hz, 4H), 8.26 (d, J=9.5 Hz, 4H), 7.57 (B of AB, d, J=17 Hz, 2H), 7.48 (A of AB, d, J=17 Hz, 2H), 7.28 (s, 2H), 7.21 (s, 2H), 7.14 (s, 2H), 4.05–3.99 (m, 12H), 1.90–1.71 (m, 12H), 1.57–1.25 (m, 60H), 0.96–0.75 ppm (m, 18H); ^{13}C NMR ($CDCl_3$): δ=151.9, 151.0, 150.3, 150.0, 147.6, 147.0, 146.9, 146.6, 146.2, 146.1, 145.9, 145.8, 145.5, 145.3, 145.2, 145.1, 144.6, 144.3, 143.9, 143.1, 142.8, 142.7, 142.3, 142.1, 141.9 (2C), 141.8, 140.6, 139.2, 137.1, 135.0, 130.3, 127.2, 125.3, 123.1, 119.1, 119.0, 116.3, 110.7, 89.3, 84.3, 69.9, 69.5, 32.2, 30.0, 29.9, 29.8, 29.7, 26.7, 26.6, 26.5, 23.0, 14.5, 14.4 ppm; IR (KBr): $\tilde{\nu}$=2925.4, 1638.6, 1616.7, 1587.6 (CH=N), 1493.0, 1328.1, 1197.1, 1022.5, 845.4, 527.7 cm^{-1}; MALDI-TOF: m/z: 2814.7, 2092.6 [M^+-C_{60}].

F-5PV-F: Yield: 10%; ^{1}H NMR ($CDCl_3$): δ=8.34 (d, J=9.5 Hz, 4H), 8.26 (d, J=9.5 Hz, 4H), 7.58 (B of AB, d, J=17 Hz, 4H), 7.48 (A of AB, d, J=17 Hz, 4H), 7.29 (s, 2H), 7.28 (s, 2H), 7.21 (s, 2H), 7.17 (s, 2H), 7.15 (s, 2H), 4.10–4.00 (m, 20H), 1.92–1.82 (m, 20H), 1.58–1.27 (m, 100H), 0.89–0.81 ppm (m, 30H); ^{13}C NMR ($CDCl_3$): δ=151.9, 150.9, 150.1, 147.6, 147.0, 146.3, 146.1, 146.0, 145.8, 145.5, 145.2, 145.1, 144.7, 144.3, 143.1, 142.9, 142.3, 142.2, 142.0, 140.7, 139.2, 137.1, 135.2, 130.4, 127.9, 126.8, 125.4, 123.3, 114.2, 110.5, 97.8, 89.3, 83.5, 69.9, 69.5, 32.2, 29.8, 29.7, 26.6, 26.5, 23.8, 23.0, 14.5, 14.4 ppm; IR (KBr): $\tilde{\nu}$=2921.3, 1636.3, 1616.5, 1588.1 (CH=N), 1495.5, 1319.9, 1262.9, 1020.9, 800.2, 527.3 cm^{-1}; MALDI-TOF: m/z: 3530.9, 2810.9 [M^+-C_{60}].

F-3PV: Yield: 58%; ^{1}H NMR ($CDCl_3$): δ=10.4 (s, 1H; CHO), 8.32 (d, J=9.5 Hz, 2H), 8.24 (d, J=9.5 Hz, 2H), 7.55–7.44 (m, 4H), 7.26 (s, 2H), 7.20 (s, 2H), 7.13 (s, 2H), 4.05–4.02 (m, 12H), 1.86–1.71 (m, 12H), 1.58–1.25 (m, 60H), 0.88–0.79 ppm (m, 18H); ^{13}C NMR ($CDCl_3$): δ=189.1 (CHO), 156.2, 152.0, 151.3, 151.1, 150.6, 150.4, 150.2, 147.7, 147.1, 147.0, 146.6, 146.3, 146.2, 146.1, 145.9, 145.6, 145.4, 145.3, 145.2, 145.1, 144.7, 144.4, 144.0, 143.2, 143.1, 143.0, 142.9, 142.8, 142.4, 142.2, 142.1, 142.0, 141.9, 140.7, 139.2, 137.1, 135.2, 130.3, 127.7, 127.0, 125.3, 125.2, 124.0, 123.0, 119.0, 116.3, 110.6, 110.0, 89.2, 84.2, 69.7, 69.3, 69.1, 69.0, 58.5, 31.8, 31.8, 31.7, 30.9, 29.7, 29.5, 29.4, 29.3, 29.2, 26.4, 26.3, 26.2, 26.1, 22.6, 18.4, 14.1, 14.0 ppm; IR (KBr): $\tilde{\nu}$=2852.5, 1733.0 (C=O), 1677.4, 1591.9 (CH=N), 1467.9, 1322.6, 1198.6, 852.3, 526.9 cm^{-1}; MALDI-TOF: m/z: 1959.8, 1239.8 [M^+-C_{60}].

F-5PV: Yield: 19%; ^{1}H NMR ($CDCl_3$): δ=10.4 (s, 1H; CHO), 8.32 (d, J=9.5 Hz, 2H), 8.26 (d, J=9.5 Hz, 2H), 7.66–7.44 (m, 8H), 7.33 (s, 2H), 7.21 (s, 2H), 7.18 (s, 2H), 7.17 (s, 2H), 7.15 (s, 2H), 4.07–4.04 (m, 20H), 1.89–1.86 (m, 20H), 1.59–1.27 (m, 100H), 0.90–0.85 ppm (m, 30H); ^{13}C NMR ($CDCl_3$): δ=189.2 (CHO), 156.2, 152.1, 152.0, 151.2, 151.1, 151.0, 150.6, 150.3, 150.2, 147.7, 147.1, 147.0, 146.4, 146.3, 146.1, 146.0, 145.9, 145.6, 145.4, 145.3, 145.2, 145.1, 145.1, 144.8, 144.7, 144.4, 144.3, 144.0, 143.8, 143.2, 143.1, 143.0, 142.9, 142.8, 142.3, 142.2, 142.1, 142.0, 141.9, 140.7, 139.2, 139.1, 137.1, 135.2, 125.3, 119.0, 110.8, 110.6, 110.5, 110.3, 110.0, 89.4, 89.2, 84.2, 69.4, 69.3, 31.9, 31.8, 31.8, 29.7, 29.5, 29.4, 29.4, 29.3, 29.3, 29.2, 26.4, 26.2, 26.1, 22.6, 14.2, 14.1, 14.0 ppm; IR (KBr): $\tilde{\nu}$=2925.3, 2850.4, 1717.3 (C=O), 1636.7, 1618.5, 1587.3 (CH=N), 1496.3, 1322.1, 1257.1, 1197.3, 802.1, 526.6 cm^{-1}; MALDI-TOF: m/z: 2676.5, 1956.5 [M^+-C_{60}].

Electrochemistry: Cyclic voltammetry measurements were carried out on an Autolab PGSTAT 30 potentiostat by using a BAS MF-2062 Ag/0.01 M $AgNO_3$, 0.1 M TBAP in ODCB (*ortho*-dichlorobenzene)/ACN (acetonitrile) reference electrode, an auxiliary electrode consisting of a Pt wire, and a Metrohm 6.0805.010 conventional glassy carbon electrode (3 mm o.d.) as a working electrode, which was directly immersed in the solution. A 10 mL electrochemical cell from BAS (Model VC-2) was also used. The reference potential was shifted by 290 mV towards a more negative potential relative to the Ag/AgCl scale. $E_{1/2}$ values were taken as the average of the anodic and cathodic peak potentials. Scan rate: 100 mV s^{-1}.

Photophysical measurements: Experimental procedures were as described previously.[19] Emission spectra were obtained with an Edinburgh FLS920 spectrometer (continuous 450 W Xe lamp), equipped with a peltier-cooled Hamamatsu R928 photomultiplier tube (185–850 nm) or a Hamamatsu R5509–72 supercooled photomultiplier tube (193 K, 800–1700 nm range). Corrected spectra were obtained on a calibration curve supplied with the instrument. Emission lifetimes were determined with the Edinburgh FLS920 spectrometer equipped with a laser diode head as excitation source (1 MHz repetition rate, λ_{exc}=407 nm, 200 ps time resolution) and the above-mentioned Hamamatsu R928 PMT as detector.

STM and SFM measurements: Scanning tunneling microscopy was performed at the solid–liquid interface employing a Multimode (Veeco) operating with a picoAmp preamplifier and 0.25 mm thick mechanically cut Pt/Ir tips. A drop of an almost saturated solution in 1,2,4-trichlorobenzene (Aldrich) was applied to the basal plane of a freshly cleaved highly oriented pyrolitic graphite (HOPG) surface. Trichlorobenzene was chosen because it possesses a low volatility which permits to carry out the STM studies for several hours at the solid–liquid interface with the STM tip immersed in the solution. Moreover it is pretty good for solubilizing conjugated molecules due to both its chlorination and its aromaticity. By changing the tunneling parameters it was possible to visualize either the organic adsorbate with a sub-molecular resolution or the HOPG substrate with atomic resolution. Typical tunneling parameters employed to visualize the organic adsorbates are bias voltage (U_t)=200–600 mV and average tunneling current (I_t)=5–15 pA. Image processing was done exploiting a commercial software SPIP version 2.000, Image Metrology ApS.

Scanning force microscope (SFM) studies in the noncontact mode[66] were carried out using an Autoprobe CP Research (Thermomicroscope) recording the height signal (output of the feedback signal). SFM was run in an air environment at room temperature with scan rates of 1–1.5 Hz per line. Images with scan lengths ranging from 60 μm down to 1 μm were recorded with a resolution of 512×512 pixels by using the 100 μm scanner and noncontact Si ultralevers with a spring constant of k in the range 2.1–17.0 N m^{-1}.

Ultra thin films for SFM analysis have been prepared by drop casting on freshly cleaved HOPG surfaces a solution of **F-5PV-F** in toluene (HPLC grade, Aldrich). Different concentrations of 5×10^{-1}, 5×10^{-3}, and to 5×10^{-5} mg mL^{-1} were used. After deposition, the solvent was removed by heating the sample for 60 min at 70 °C.

Acknowledgements

We thank the European Commission for financial support through the RTN project FAMOUS (Contract HPRN-CT-2002–00171). We also thank Italian MIUR (contract FIRB RBNE019H9K, Molecular Manipulation for Nanometric Machines), the ESF-SONS-BIONICS project, the Spanish Ministry of Education and Science (Proyect CTQ2004–00364/BQU) and Feder funds.

[1] H. Imahori, Y. Sakata, *Eur. J. Org. Chem.* **1999**, 2445–2457.
[2] D. M. Guldi, *Chem. Commun.* **2000**, 321–327.
[3] D. Gust, T. A. Moore, A. L. Moore, *Acc. Chem. Res.* **2001**, *34*, 40–48.
[4] G. Yu, J. Gao, J. C. Hummelen, F. Wudl, A. J. Heeger, *Science* **1995**, *270*, 1789–1791.
[5] A. Cravino, N. S. Sariciftci, *J. Mater. Chem.* **2002**, *12*, 1931–1943.
[6] J. K. J. van Duren, X. N. Yang, J. Loos, C. W. T. Bulle-Lieuwma, A. B. Sieval, J. C. Hummelen, R. A. J. Janssen, *Adv. Funct. Mater.* **2004**, *14*, 425–434.
[7] N. Armaroli, *Photochem. Photobiol. Sci.* **2003**, *2*, 73–87.
[8] J. F. Nierengarten, *New J. Chem.* **2004**, *28*, 1177–1191.
[9] J. F. Nierengarten, *Sol. Energy Mater. Sol. Cells* **2004**, *83*, 187–199.
[10] H. Imahori, K. Hagiwara, T. Akiyama, M. Aoki, S. Taniguchi, T. Okada, M. Shirakawa, Y. Sakata, *Chem. Phys. Lett.* **1996**, *263*, 545–550.
[11] M. Carano, T. Da Ros, M. Fanti, K. Kordatos, M. Marcaccio, F. Paolucci, M. Prato, S. Roffia, F. Zerbetto, *J. Am. Chem. Soc.* **2003**, *125*, 7139–7144.

[12] F. Langa, P. de la Cruz, J. L. Delgado, M. J. Gomez-Escalonilla, A. Gonzalez-Cortes, A. de la Hoz, V. Lopez-Arza, *New J. Chem.* **2002**, *26*, 76–80.
[13] M. Prato, Q. C. Li, F. Wudl, V. Lucchini, *J. Am. Chem. Soc.* **1993**, *115*, 1148–1150.
[14] D. M. Guldi, S. Gonzalez, N. Martin, A. Anton, J. Garin, J. Orduna, *J. Org. Chem.* **2000**, *65*, 1978–1983.
[15] T. Da Ros, M. Prato, M. Carano, P. Ceroni, F. Paolucci, S. Roffia, *J. Am. Chem. Soc.* **1998**, *120*, 11645–11648.
[16] N. Martin, L. Sanchez, B. Illescas, I. Perez, *Chem. Rev.* **1998**, *98*, 2527–2547.
[17] F. Langa, P. de la Cruz, E. Espildora, A. de la Hoz, J. L. Bourdelande, L. Sanchez, N. Martin, *J. Org. Chem.* **2001**, *66*, 5033–5041.
[18] P. de la Cruz, A. Diaz-Ortiz, J. J. Garcia, M. J. Gomez-Escalonilla, A. de la Hoz, F. Langa, *Tetrahedron Lett.* **1999**, *40*, 1587–1590.
[19] N. Armaroli, G. Accorsi, J. P. Gisselbrecht, M. Gross, V. Krasnikov, D. Tsamouras, G. Hadziioannou, M. J. Gomez-Escalonilla, F. Langa, J. F. Eckert, J. F. Nierengarten, *J. Mater. Chem.* **2002**, *12*, 2077–2087.
[20] D. M. Guldi, C. P. Luo, A. Swartz, R. Gomez, J. L. Segura, N. Martin, *J. Phys. Chem. A* **2004**, *108*, 455–467.
[21] J. F. Eckert, J. F. Nicoud, J. F. Nierengarten, S. G. Liu, L. Echegoyen, F. Barigelletti, N. Armaroli, L. Ouali, V. Krasnikov, G. Hadziioannou, *J. Am. Chem. Soc.* **2000**, *122*, 7467–7479.
[22] E. Peeters, P. A. van Hal, J. Knol, C. J. Brabec, N. S. Sariciftci, J. C. Hummelen, R. A. J. Janssen, *J. Phys. Chem. B* **2000**, *104*, 10174–10190.
[23] D. M. Guldi, A. Swartz, C. P. Luo, R. Gomez, J. L. Segura, N. Martin, *J. Am. Chem. Soc.* **2002**, *124*, 10875–10886.
[24] E. H. A. Beckers, P. A. van Hal, A. Schenning, A. El-ghayoury, E. Peeters, M. T. Rispens, J. C. Hummelen, E. W. Meijer, R. A. J. Janssen, *J. Mater. Chem.* **2002**, *12*, 2054–2060.
[25] E. H. A. Beckers, P. A. van Hal, A. Dhanabalan, S. C. J. Meskers, J. Knol, J. C. Hummelen, R. A. J. Janssen, *J. Phys. Chem. A* **2003**, *107*, 6218–6224.
[26] M. Gutierrez-Nava, G. Accorsi, P. Masson, N. Armaroli, J. F. Nierengarten, *Chem. Eur. J.* **2004**, *10*, 5076–5086.
[27] T. Gu, D. Tsamouras, C. Melzer, V. Krasnikov, J. P. Gisselbrecht, M. Gross, G. Hadziioannou, J. F. Nierengarten, *ChemPhysChem* **2002**, *3*, 124–127.
[28] S. Knorr, A. Grupp, M. Mehring, G. Grube, F. Effenberger, *J. Chem. Phys.* **1999**, *110*, 3502–3508.
[29] P. A. van Hal, E. H. A. Beckers, S. C. J. Meskers, R. A. J. Janssen, B. Jousselme, P. Blanchard, J. Roncali, *Chem. Eur. J.* **2002**, *8*, 5415–5429.
[30] H. Kanato, K. Takimiya, T. Otsubo, Y. Aso, T. Nakamura, Y. Araki, O. Ito, *J. Org. Chem.* **2004**, *69*, 7183–7189.
[31] T. Nakamura, M. Fujitsuka, Y. Araki, O. Ito, J. Ikemoto, K. Takimiya, Y. Aso, T. Otsubo, *J. Phys. Chem. B* **2004**, *108*, 10700–10710.
[32] J. L. Segura, R. Gomez, N. Martin, C. P. Luo, D. M. Guldi, *Chem. Commun.* **2000**, 701–702.
[33] Y. Obara, K. Takimiya, Y. Aso, T. Otsubo, *Tetrahedron Lett.* **2001**, *42*, 6877–6881.
[34] J. J. Apperloo, C. Martineau, P. A. van Hal, J. Roncali, R. A. J. Janssen, *J. Phys. Chem. A* **2002**, *106*, 21–31.
[35] C. Martineau, P. Blanchard, D. Rondeau, J. Delaunay, J. Roncali, *Adv. Mater.* **2002**, *14*, 283-+.
[36] K. I. Yamanaka, M. Fujitsuka, Y. Araki, O. Ito, T. Aoshima, T. Fukushima, T. Miyashi, *J. Phys. Chem. A* **2004**, *108*, 250–256.
[37] N. Negishi, K. Takimiya, T. Otsubo, Y. Harima, Y. Aso, *Chem. Lett.* **2004**, *33*, 654–655.
[38] N. Armaroli, F. Barigelletti, P. Ceroni, J. F. Eckert, J. F. Nicoud, J. F. Nierengarten, *Chem. Commun.* **2000**, 599–600.
[39] G. Accorsi, N. Armaroli, J. F. Eckert, J. F. Nierengarten, *Tetrahedron Lett.* **2002**, *43*, 65–68.
[40] J. F. Nierengarten, N. Armaroli, G. Accorsi, Y. Rio, J. F. Eckert, *Chem. Eur. J.* **2003**, *9*, 37–41.
[41] F. Cacialli, J. S. Wilson, J. J. Michels, C. Daniel, S. C. , R. H. Friend, N. Severin, P. Samorì, J. P. Rabe, M. J. O'Connell, P. N. Taylor, H. L. Anderson, *Nat. Mater.* **2002**, *1*, 160–164.
[42] S. Z. Kang, S. L. Xu, H. M. Zhang, L. B. Gan, C. Wang, L. J. Wan, C. L. Bai, *Surf. Sci.* **2003**, *536*, L408–L414.
[43] K. Yase, N. Ara-Kato, T. Hanada, H. Takiguchi, Y. Yoshida, G. Back, K. Abe, N. Tanigaki, *Thin Solid Films* **1998**, *331*, 131–140.
[44] Y. Kim, L. Jiang, T. Iyoda, K. Hashimoto, A. Fujishima, *Surf. Sci.* **1997**, *385*, L945–L951.
[45] T. Sakurai, X. D. Wang, Q. K. Xue, Y. Hasegawa, T. Hashizume, H. Shinohara, *Prog. Surf. Sci.* **1996**, *51*, 263–408.
[46] P. Byszewski, Z. Klusek, S. Pierzgalski, S. Datta, E. Kowalska, M. Poplawska, *J. Electron Spectrosc. Relat. Phenom.* **2003**, *130*, 25–32.
[47] M. de Wild, S. Berner, H. Suzuki, H. Yanagi, D. Schlettwein, S. Ivan, A. Baratoff, H. J. Guentherodt, T. A. Jung, *ChemPhysChem* **2002**, *3*, 881–885.
[48] D. Bonifazi, H. Spillmann, A. Kiebele, M. de Wild, P. Seiler, F. Y. Cheng, H. J. Guntherodt, T. Jung, F. Diederich, *Angew. Chem.* **2004**, *116*, 4863–4867; *Angew. Chem. Int. Ed.* **2004**, *43*, 4759–4763.
[49] M. J. Han, L. J. Wan, S. B. Lei, H. M. Li, X. L. Fan, C. L. Bai, Y. L. Li, D. B. Zhu, *J. Phys. Chem. B* **2004**, *108*, 965–970.
[50] M. J. Gomez-Escalonilla, F. Langa, J. M. Rueff, L. Oswald, J. F. Nierengarten, *Tetrahedron Lett.* **2002**, *43*, 7507–7511.
[51] J. F. Nierengarten, T. Gu, G. Hadziioannou, D. Tsamouras, V. Krasnikov, *Helv. Chim. Acta* **2004**, *87*, 2948–2966.
[52] H. Detert, D. Schollmeyer, E. Sugiono, *Eur. J. Org. Chem.* **2001**, 2927–2938.
[53] J. L. Delgado, P. de la Cruz, V. Lopez-Arza, F. Langa, D. B. Kimball, M. M. Haley, Y. Araki, O. Ito, *J. Org. Chem.* **2004**, *69*, 2661–2668.
[54] E. Espildora, J. L. Delgado, P. de la Cruz, A. de la Hoz, V. Lopez-Arza, F. Langa, *Tetrahedron* **2002**, *58*, 5821–5826.
[55] Hyperchem 5.1 Package
[56] U. Mazzucato, F. Momicchioli, *Chem. Rev.* **1991**, *91*, 1679–1719.
[57] E. Peeters, A. M. Ramos, S. C. J. Meskers, R. A. J. Janssen, *J. Chem. Phys.* **2000**, *112*, 9445–9454.
[58] A. Gesquière, P. Jonkheijm, A. Schenning, E. Mena-Osteritz, P. Bäuerle, S. De Feyter, F. C. De Schryver, E. W. Meijer, *J. Mater. Chem.* **2003**, *13*, 2164–2167.
[59] S. Uemura, P. Samorì, M. Kunitake, C. Hirayama, J. P. Rabe, *J. Mater. Chem.* **2002**, *12*, 3366–3367.
[60] R. Lazzaroni, A. Calderone, J. L. Brédas, J. P. Rabe, *J. Chem. Phys.* **1997**, *107*, 99–105.
[61] Y. Z. Li, M. Chander, J. C. Patrin, J. H. Weaver, L. P. F. Chibante, R. E. Smalley, *Phys. Rev. B* **1992**, *45*, 13837–13840.
[62] C. A. Hunter, K. R. Lawson, J. Perkins, C. J. Urch, *J. Chem. Soc. Perkin Trans. 2* **2001**, 651–669.
[63] P. Samorí, A. Fechtenkotter, F. Jäckel, T. Bohme, K. Müllen, J. P. Rabe, *J. Am. Chem. Soc.* **2001**, *123*, 11462–11467.
[64] V. Georgakilas, F. Pellarini, M. Prato, D. M. Guldi, M. Melle-Franco, F. Zerbetto, *Proc. Natl. Acad. Sci. USA* **2002**, *99*, 5075–5080.
[65] P. Samorì, M. Keil, R. Friedlein, J. Birgerson, M. Watson, M. Müllen, W. R. Salaneck, J. P. Rabe, *J. Phys. Chem. B* **2001**, *105*, 11114–11119.
[66] P. Samorì, J. P. Rabe, *J. Phys. Condens. Matter* **2002**, *14*, 9955.

Received: January 25, 2005
Published online: April 29, 2005

